9th International Conference on Numerical Ship Hydrodynamics
Ann Arbor, Michigan, August 5-8, 2007

Large Amplitude Body Motion Computations in the Time-Domain

Xinshu Zhang, Piotr Bandyk and Robert F. Beck *
Dept. of Naval Architecture and Marine Engineering
University of Michigan, Ann Arbor, MI 48109

Abstract

Large amplitude, time-domain, wave-body interactions are studied in this paper for problems with forward speed. Both two-dimensional strip theory and three-dimensional computation methods are shown and compared by a number of numerical simulations. In the present approach, an exact body boundary condition and linearized free surface boundary conditions are used. By distributing desingularized sources above the calm water surface and using constant-strength flat panels on the exact body surface, the boundary integral equations are solved numerically at each time step. Once the fluid velocities on the free surface are computed, the free surface elevation and potential are updated by integrating the free surface boundary conditions. After each time step, the body surface and free surface are regrided due to the instantaneous changing wetted body geometry. The desingularized source method applied on the free surface produces non-singular kernels in the integral equations by moving the fundamental singularities a small distance outside of the fluid domain. Constant-strength flat panels are used to model bodies with any arbitrary shape.

Extensive results are presented to validate the efficiency of the present methods. These results include the added mass and damping computations for a modified Wigley hull and a S-175 hull with forward speed using both two-dimensional and three-dimensional approaches. Heave force and pitch moment time histories of a S-175 hull due to a heave motion using a time-domain body-exact strip theory are presented. Diffraction forces acting on a modified Wigley hull due to a linear head sea incoming wave using fully three-dimensional method are also obtained. All the computational results are compared with experiments or other numerical solutions.

1 INTRODUCTION

The accurate prediction of wave-induced motions and loads are very important in ship and offshore design, which requires knowledge of the maximum value of various design parameters such as ship motion amplitude, bending moments, impact forces, etc.

A mixed Euler-Lagrange time-stepping scheme (MEL) was first introduced by Longuet-Higgins & Cokelet (1976) for solving two-dimensional fully nonlinear water wave problems. Since then, MEL methods have also been successfully used to solve fully nonlinear, three-dimensional wave and wave-body interaction problems (Dommermuth & Yue,1987; Xue et al., 2001; Cao, Schultz & Beck,1990, 1991; Cao, 1991; Cao, Lee & Beck, 1992; Scorpio et al., 1996). The problems with MEL computations are the instabilities of the free surface and wave breaking. The instabilities can often be eliminated by improved numerical techniques, but wave breaking is a natural phenomenon that is expected to occur in any large body motion or wave situation. Computations normally are forced to stop when wave breaking occurs. Various techniques have been proposed to continue the computations after wave breaking, but they are still not robust and can lead to nonphysical solutions.

A compromise between fully nonlinear computations and linear theory is the so-called body-exact approach. In the body-exact problem, the body boundary condition is satisfied on the instantaneous wetted surface of the body while the linearized free surface boundary conditions are retained. In order to solve for the hydrodynamic forces due to large body motions in the body-exact problem, a time-domain approach is preferred. A method to deal with the exact body boundary condition using a time-domain free surface Green function has been developed by Beck & Magee (1990) for a submerged body performing arbitrary motions. Other researchers such as Lin & Yue (1990) also have successfully obtained results for a surface-piercing body problem using the time-domain free surface Green function method.

In order to develop computationally fast seakeeping calculations, but still retaining the important nonlinearities, a time-domain body-exact method using Rankine sources has been developed. Earlier work on two-dimensional body-exact computations has been given by Zhang and Beck (2006, 2007). They solved two-dimensional large amplitude radiation and diffraction problems including water entry and exit. Com-

*Address all correspondence to this author.

parisons with the other numerical calculations and experiments were good.

In this paper, we have continued to develop two-dimensional and three-dimensional, body-exact computational models together with using a Rankine source Green function to compute the large amplitude body motions in waves. The exact body boundary condition is applied on the instantaneous wetted hull surface under $z = 0$. For the large amplitude computations, the instantaneous submerged body surface is repanelized at each time step to capture the nonlinearities due to the changing geometry. The linearized free surface boundary conditions are used.

To compute the three-dimensional problem results, two approaches have been followed. The first is a strip theory in which a series of two-dimensional problems at different cross-sections are solved at each time step. Once the boundary value problems have been solved at each section, Radial Basis Functions (RBF) are used to compute the longitudinal derivatives of the velocity potential on the body surface. In the second approach, the three-dimensional problem is solved completely and the derivative of the velocity potential on body is computed directly. For the large amplitude radiation problem with forward speed, both methods are used to compute the hydrodynamic forces, and both sets of results are compared with experiments.

As will be formulated in the following sections, the three-dimensional solver includes the forward speed effects both in the free surface boundary conditions and the pressure calculations. The derivatives of the potential on the hull can be easily computed once the source strengths have been obtained by solving the boundary value problem. In the strip theory calculations, the boundary value problem is solved at different cross-sections and the forward speed correction is only included in the pressure computations by computing the derivative of potential in the x-direction on the hull using Radial Basis Functions. The computation time in solving the three-dimensional problem is relatively more expensive than solving the problem using a time-domain strip theory. The accuracy of those results will be shown and compared in the following sections.

2 MATHEMATICAL FORMULATION

2.1 Three-Dimensional

A boundary value problem for a vessel travelling in deep water is solved. The vessel moves with forward speed $\vec{U}(t)$, and may be undergoing unsteady oscillations in its six degrees of freedom. The fluid is assumed to be ideal and the flow irrotational. Two coordinates systems will be employed: the $\vec{x_o}$ system is fixed in space, and $\vec{x}$ system is fixed to the mean position of the ship and is moving with forward speed $\vec{U}(t)$ along the track of the ship. The boundary value problem is solved in the right hand moving coordinate system

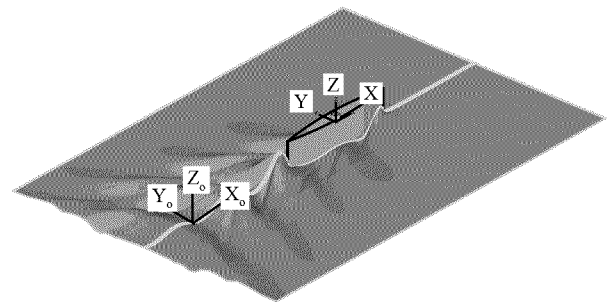

Figure 1: Problem sketch and reference frames

(x, y, z), as shown in Figure 1. The x-axis points out the bow, and the z-axis upward. The origin is at the calm water line at mid-ship.

A velocity potential is introduced to describe the fluid motion by using the above assumptions such that the fluid velocity can be expressed as the gradient of potential function, $\vec{V}(\vec{x}, t) = \nabla\Phi = \nabla(-U(t)x + \phi(x, y, z, t))$, where ϕ is the perturbation velocity potential.

The form of the linearized free surface boundary conditions are:

$$\frac{\partial \eta}{\partial t} = \frac{\partial \phi}{\partial z} + \vec{U} \cdot \nabla\eta \quad (1)$$

$$\frac{\partial \phi}{\partial t} = -g\eta + \vec{U} \cdot \nabla\phi - \frac{P_a}{\rho} \quad (2)$$

In order to use an Euler-Lagrange free surface time stepping scheme, the free surface boundary conditions can be rewritten in a more convenient form:

$$\frac{\delta \eta}{\delta t} = \frac{\partial \phi}{\partial z} + \vec{U} \cdot \nabla\eta + \vec{v} \cdot \nabla\eta \quad (3)$$

$$\frac{\delta \phi}{\delta t} = -g\eta + \vec{U} \cdot \nabla\phi - \frac{P_a}{\rho} + \vec{v} \cdot \nabla\phi \quad (4)$$

where $\frac{\delta}{\delta t} = \frac{\partial}{\partial t} + \vec{v} \cdot \nabla$ is the time derivative following a fluid particle along a prescribed path. The velocity of the particle in moving coordinate system is $\vec{v} = (u, v, 0)$. Here, u and v are the prescribed velocities for the horizontal plane motion of the free surface collocation points. u is allowed to move with the translation velocity $-U$, and v is prescribed so that collocation points move on the given paths around the body.

This formulation has the desired effect of restricting collocation points from passing through the body boundary. An alternative free surface boundary condition would be to set $\vec{v} = (0, 0, 0)$, using equations (1)

and (2). In this case $\frac{\delta\eta}{\delta t} = \frac{\partial\eta}{\partial t}$ and the collocation points are fixed on the calm water surface, tracking the free surface elevations at points in the $x-y$ plane like wave probes. The advantage of this scheme is that no regriding of the free surface after each time step is required if the body is wall-sided. The disadvantage is that the free surface slope, $\nabla\eta$, must be computed numerically. $\nabla\eta$ may be difficult to compute accurately in a three-dimensional problem, especially at the boundaries of the free surface domain where one sided differencing must be used. The free surface/body intersection line is where this problem would be most detrimental.

All the velocity potentials should satisfy the Laplace equation under the assumption of ideal potential flow. By applying Green's theorem and using a Rankine source Green function, the velocity potential can be written as

$$\phi = \int\int_{S_F \cup S_B} G(\vec{x},\vec{\xi})\sigma(\vec{\xi})ds \tag{5}$$

where $G = \frac{1}{r(\vec{x},\vec{\xi})}$; σ is the source strength on the boundary; S_F is the calm water free surface; and $S_B(t)$ is the instantaneous wetted body surface. The exact body boundary condition is

$$\vec{n}\cdot\nabla\phi = U_o(t)n_1(t) + V_H\cdot\vec{n}(t) \qquad on \quad S_B(t) \tag{6}$$

where $U_o(t)$ is the time-dependent translating velocity of the body in the x direction; $\vec{n}$ is the inward unit normal on the body surface(out of fluid); n_1 is the component of unit normal in the x direction; and V_H is the motion velocity including rotational modes of a point on the ship surface.

The perturbation potential ϕ must satisfy the radiation boundary condition such that there must be no incoming waves and, in the deep water problem, ϕ vanishes as $z \to -\infty$. The initial conditions at $t = 0$ can be written as:

$$\phi = \phi_t = 0 \quad \text{in the fluid domain} \tag{7}$$

After solving the boundary value problem, the force and moment can be determined by using:

$$\vec{F} = \int\int_{S_{B(t)}} p\vec{n}ds \tag{8}$$

$$\vec{M} = \int\int_{S_{B(t)}} p(\vec{r}\times\vec{n})ds \tag{9}$$

2.2 Two-Dimensional Strip Theory

The three-dimensional seakeeping problem can be approximated by solving a series of two-dimensional problems at cross-sections (stations) of the vessel. This is valid for long and slender ships. The two-dimensional approach used here is based on the work of Zhang and Beck (2007). The method follows the same conventions as described for the three-dimensional case. The two-dimensional flow at each station can be described by a velocity potential $\psi(y,z,t)$. In the fluid domain, ψ satisfies Laplace's equation

$$\nabla^2\psi = 0 \tag{10}$$

On the mean free surface, the linearized free surface boundary conditions are imposed

$$\zeta_t - \psi_z = 0 \qquad \text{on} \quad z = 0 \tag{11}$$

$$\psi_t + g\zeta = 0 \qquad \text{on} \quad z = 0 \tag{12}$$

where $z = \zeta(y,t)$ is the free surface elevation, g is the acceleration due to gravity. On the *instantaneous* body boundary, no normal flux is permitted

$$\frac{\partial\psi}{\partial\mathbf{N}} = V_N + U_o tan(\eta_5)N_3 - U_o tan(\eta_6)N_2 \quad \text{on} \quad S_B \tag{13}$$

where $\mathbf{N}$ is the two-dimensional unit normal vector, and is positive out of the fluid. V_N is the instantaneous velocity in the normal direction including rotational effects. The last two terms are two-dimensional corrections when there is a non-zero pitch angle, η_5, or non-zero yaw angle, η_6. In the far field, a radiation boundary condition is imposed such that there are no incoming waves; also, the water is assumed deep and the potential vanishes as $z \to -\infty$. The initial conditions at $t = 0$ are

$$\psi = \psi_t = 0 \quad \text{in the fluid domain} \tag{14}$$

At each time step a mixed boundary value problem must be solved; the potential is given on the free surface and the normal derivative of the potential is known on the body surface. In terms of the desingularized sources (as described in the next section) above the free surface and sources distributed on the body surface, the potential at any point in the fluid domain can be given

$$\psi(\mathbf{x}) = \sum_{i=1}^{N}\sigma(\xi_i)\ln|\mathbf{x}-\xi_i| + \int_{S_B}\sigma(\xi)G(\mathbf{x};\xi)dl \tag{15}$$

where S_B represent the instantaneous wetted body surface. $|\mathbf{x}-\xi_\mathbf{i}|$ represents the distance between any point in the fluid domain and the desingularized source point. $G(\mathbf{x};\xi)$ is a Rankine source Green function

$$G(\mathbf{x};\xi) = \ln r \tag{16}$$

$$r = |\mathbf{x}-\xi| \tag{17}$$

where r is the distance between a source point and a collocation point; ξ is the source point on the body boundary.

Once the source strengths are found, ψ can be evaluated by (15), and the velocity on the body $\nabla\psi$ can been obtained. The total pressure is given by Bernoulli's equation

$$p = -\rho(\frac{\partial\psi}{\partial t} + \frac{1}{2}|\nabla\psi|^2 - U_o\frac{\partial\psi}{\partial x} + gz) \tag{18}$$

Under the slender body assumption, the forces acting on the body can be approximated by integrating (18) over the instantaneous submerged body surface, which can be written as

$$\mathbf{F} = \int_L dx \int p\mathbf{N}\, dl \tag{19}$$

$$\mathbf{M} = \int_L dx \int p(\mathbf{rxN})\, dl \tag{20}$$

3 NUMERICAL METHODS

3.1 Three-Dimensional

We distribute the desingularized sources above the calm water surface. The desingularized distance is calculated according to the formula $D_s = L_d S^{\frac{1}{2}}$ (Lee, 1992), where D_s is the desingularized distance, S is the local grid area, and $L_d = 1$ is a desingularized parameter. Constant-strength flat panels are used on the body surface. The instantaneous submerged body surface is discretized into N quadrilateral elements over which the source strength is assumed constant. The nonplanar quadrilaterals are mapped to planar elements by fitting the corner points in a least-squares sense (Hess and Smith, 1964; Newman, 1986). A boundary integral equation can be solved for the unknown panel and isolated source strengths.

$$\begin{aligned}
&\sum_{j=1,j\neq i}^{M} \int_{S_j} \sigma_j \vec{n}_i \cdot \nabla_{\vec{x}_i} \frac{1}{|\vec{x}_i - \vec{\xi}_j|} ds + 2\pi\sigma_i \\
&+\sum_{j=M+1}^{N} \sigma_j \vec{n}_i \cdot \nabla_{\vec{x}_i} \frac{1}{|\vec{x}_i - \vec{\xi}_j|} = U_o(t) n_1(t) + V_H \cdot \vec{n}_i(t) \\
&\vec{x}_i \in S_B, i = 1 \cdots M \\
&\sum_{j=1}^{M} \int_{S_j} \frac{\sigma_j}{|\vec{x}_i - \vec{\xi}_j|} ds + \sum_{j=M+1}^{N} \frac{\sigma_j}{|\vec{x}_i - \vec{\xi}_j|} = \phi_{o_i} \\
&\vec{x}_i \in S_f, i = M+1 \cdots N
\end{aligned} \tag{21}$$

where

$\vec{x}_i$	$= (x_i, y_i, z_i)$, a collocation point
$\vec{n}_i$	$= (n_{x_i}, n_{y_i}, n_{z_i})$, unit normal pointing into body
S_j	= a panel integration surface on the body
M	= number of panels on the body surface
N	= total number of unknown source strengths

When the above summations (21) are applied at N collocation points ($\vec{x}_i$), an $N \times N$ linear system results,

$$A_{ij}\sigma_j = b_i \tag{22}$$

where the influence matrix $A_{ij} = G_{ij} = 1/(|\vec{x}_i - \vec{\xi}_j|)$ for collocation points on the free surface and $A_{ij} = \vec{n}_i \cdot \nabla_{\vec{x}_i} G_{ij}$ for collocation points on solid boundaries; σ_j is the vector of unknown source strengths. b_i is the vector of boundary conditions, $b_i = \phi_{o_i}$ on the free surface, $b_i = U_o(t)n_1(t) + V_H \cdot \vec{n}(t)$ on the wetted body surface.

Once the source strengths are known, the particle velocities on the free surface can be computed. Then the free surface conditions are updated by using a 4^{th}-order Runge-Kutta scheme. Meanwhile, the velocity potential on the body surface can also be obtained. By using a central time differencing scheme, the pressure acting on the body can be calculated so that the force can be obtained by integrating the pressure over the instantaneous wetted surface. The pressure on the body surface is given by the Bernoulli's equation

$$p = -\rho[\frac{\partial\phi}{\partial t} - U\frac{\partial\phi}{\partial x} + \frac{1}{2}((\frac{\partial\phi}{\partial x})^2 + (\frac{\partial\phi}{\partial y})^2 + (\frac{\partial\phi}{\partial z})^2) + gz] \tag{23}$$

The dynamic forces acting on the ship in mode j due to a unit motion in mode k can be found by integrating the consequent pressure over the instantaneous submerged body surface.

$$\begin{aligned}
F_{jk} \;=\; & \rho \int\int_{S_B} dS[-\frac{\partial\phi_k}{\partial t} + U\frac{\partial\phi_k}{\partial x} - \\
& \frac{1}{2}((\frac{\partial\phi_k}{\partial x})^2 + (\frac{\partial\phi_k}{\partial y})^2 + (\frac{\partial\phi_k}{\partial z})^2)]n_j
\end{aligned} \tag{24}$$

In this paper, we compute the derivatives of the velocity potential on the hull directly.

3.2 Two-Dimensional Strip Theory

3.2.1 Body and Free Surface Modeling

Applying the boundary conditions and using equation (15), the following integral equations can be solved to determine the unknown source strength.

$$\sum_{\Gamma_F} \sigma(\xi_i) \ln|\mathbf{x_c} - \xi_\mathbf{i}| + \int_{\Gamma_B} \sigma(\xi) G(\mathbf{x_c}, \xi) dl = \psi(\mathbf{x}_c) \quad \mathbf{x}_c \in \Gamma_F \tag{25}$$

$$\sum_{\Gamma_F} \sigma(\xi_i) \frac{\partial \ln|\mathbf{x_c} - \xi_\mathbf{i}|}{\partial n} + \int_{\Gamma_B} \sigma(\xi) \frac{\partial G(\mathbf{x_c}, \xi)}{\partial n} dl = \chi(\mathbf{x}_c) \quad \mathbf{x}_c \in \Gamma_B \tag{26}$$

where

ξ_i	= a source point
$\mathbf{x}_c$	= a point on the real boundary
χ	= the given normal velocity on the body
ψ	= the given potential on the free surface
Γ_F	= the free surface
Γ_B	= surfaces on which χ is known

The integral mixed boundary value equations, (25) and (26), can be discretized to form a system of linear

equations. On the free surface, desingularized sources are distributed outside of the domain such that the the source points never coincide with collocation or node points, avoiding singularities. Isolated sources are used rather than a distribution, reducing the complexity of the influence matrix. The desingularized distance is given by the square root of the local mesh size.

The free surface is broken up into an inner and outer region. The inner region spans four wavelengths on either side of the body, where the wavelength is given by the dispersion relation, $\lambda = \frac{2\pi g}{\omega^2}$, given a frequency of oscillation, ω. To resolve the radiated waves, 30 nodes are distributed per wavelength in the inner region. The outer region acts as a numerical beach to prevent wave reflection. 20 nodes are distributed over 80 wavelengths with exponentially increasing spacing, as determined by Lee (1992).

The body surface is modeled using panels, which are more suitable for arbitrarily shaped bodies. The resulting discretized mixed boundary value equations are given by

$$\sum_{j=1}^{N_F} \sigma_j^F \ln|\mathbf{x}_{c_i}^F - \boldsymbol{\xi}_{s_j}^F| + \sum_{j=1}^{N_B} \sigma_j^B \int_{\Delta l_j} \ln|\mathbf{x}_{c_i}^F - \boldsymbol{\xi}_j^B| dl = \psi(\mathbf{x}_{c_i}^F) \tag{27}$$

$$\begin{aligned} &-\pi\sigma_i^B + \sum_{j=1}^{N_F} \frac{\sigma_j^F (\mathbf{x}_{c_i}^B - \boldsymbol{\xi}_{s_j}^F) \cdot \mathbf{n}_{x_{c_i}}}{|\mathbf{x}_{c_i}^B - \boldsymbol{\xi}_{s_j}^F|^2} + \\ &\sum_{j=1, j\neq i}^{N_B} \sigma_j^B \int_{\Delta l_j} \frac{(\mathbf{x}_{c_i}^B - \boldsymbol{\xi}_j^B) \cdot \mathbf{n}_{x_{c_i}}}{|\mathbf{x}_{c_i}^B - \boldsymbol{\xi}_j^B|^2} dl = \chi(\mathbf{x}_{c_i}^B) \end{aligned} \tag{28}$$

In matrix form, equations (27) and (28) are solved using LU decomposition. Once the source strengths are known, the fluid velocity on the free surface and pressure on the exact body can be computed.

3.2.2 Time Evolution

The body is repanelized at each time step using a "rubber band" technique. The number of panels remains the same for each station, and they are stretched to where the exact body intersects the calm water surface, $z = 0$. This requires a correction in the $\partial\psi/\partial t$ term in equation (18), such that

$$(\frac{\partial\psi}{\partial t})^t = (\frac{\delta\psi}{\delta t})^t - v^t \cdot \nabla\psi^t = (\frac{\psi^t - \psi^{t-\Delta t}}{\Delta t}) - v^t \cdot \nabla\psi^t \tag{29}$$

where ψ^t is the velocity potential at time step t, and v^t is the moving node velocity due to repanelization.

The free surface elevation and potential are updated using the kinematic (11) and dynamic (12) free surface boundary conditions. Time stepping is done using a 3rd-order Adams-Bashforth scheme as shown below.

$$\begin{aligned} \zeta^{t+\Delta t} &= \zeta^t - \frac{\Delta t}{12}[23(\frac{\partial\zeta}{\partial t})^t - 16(\frac{\partial\zeta}{\partial t})^{t-\Delta t} + \\ &\quad 5(\frac{\partial\zeta}{\partial t})^{t-2\Delta t}] \end{aligned} \tag{30}$$

$$\begin{aligned} \psi^{t+\Delta t} &= \psi^t - \frac{\Delta t}{12}[23(\frac{\partial\psi}{\partial t})^t - 16(\frac{\partial\psi}{\partial t})^{t-\Delta t} + \\ &\quad 5(\frac{\partial\psi}{\partial t})^{t-2\Delta t}] \end{aligned} \tag{31}$$

The updated free surface and potentials are used to start the mixed boundary value problem at the next time step. To ensure consistent free surface resolution in time, the free surface nodes are relocated to a distribution consistent with the original distribution (based on the location of the body intersecting the free surface). The values of ζ and ψ are interpolated using cubic splines to the new distribution.

3.2.3 Section Exit and Entry

One of the main reasons for using the body-exact approach is the ability to get accurate solutions for large-amplitude motions, which are non-linear. This includes allowing sections to come out of and go back into the water. This is done simply by stopping calculations as a section comes out of the water, then re-initializing ψ and ψ_t to zero at that section. As the section enters the water, the two-dimensional problem is solved as usual. The velocity potentials are used in pressure calculations only after the solution steadies, after three time steps.

3.2.4 Forward Speed Corrections

To solve the full three-dimensional problem with forward speed, classical strip theory needs a correction for the the interaction between sections along the longitudinal direction. With non-zero forward speed, the pressure equation (18), including the moving node correction, becomes

$$p = -\rho(\frac{\delta\psi}{\delta t} + \frac{1}{2}|\nabla\psi|^2 - U_o\frac{\partial\psi}{\partial x} - v \cdot \nabla\psi + gz) \tag{32}$$

There is a necessity to find the $\partial\psi/\partial x$ term in the pressure calculation when there is a non-zero forward speed. The method implemented here is the use of radial basis functions. This can only be done once the two-dimensional problem is solved at each section. The velocity potentials on the body must be known at each section. The details of this method are discussed in the following section.

3.2.5 Radial Basis Functions

The forward speed problem can be solved by using a radial basis function (RBF) to approximate the $\partial\psi/\partial x$ term in the pressure calculation. Using this method to numerically solve partial differential equations is discussed by Kansa (1999). A more general discussion of RBFs is presented by Buhmann (2000).

Once the two-dimensional problem is solved for each section, the velocity potentials at nodes on the entire body are given as a function of the Euclidean distance between the nodes.

$$g_j(\mathbf{x}) \equiv g(||\mathbf{x} - \mathbf{x}_j||) \tag{33}$$

$$\psi(\mathbf{x}_i) = \sum_{j=1}^{N} \alpha_j g_j(\mathbf{x}_i) + \alpha_{N+1} \tag{34}$$

$$\sum_{j=1}^{N} \alpha_j = 0 \tag{35}$$

where g is one of many possible basis functions. The final equation (35) for the coefficients α_j is to ensure uniqueness. These expansion coefficients are found by setting up a system of $N+1$ equations, such that

$$P = \begin{bmatrix} 1 \\ \vdots \\ 1 \end{bmatrix} \in \mathbf{R^N}$$

$$G = \begin{bmatrix} g_1(\mathbf{x}_1) & \dots & g_N(\mathbf{x}_1) \\ \vdots & g_j(\mathbf{x}_i) & \vdots \\ g_1(\mathbf{x}_N) & \dots & g_N(\mathbf{x}_N) \end{bmatrix} \in \mathbf{R^{NxN}}$$

$$H = \begin{bmatrix} G & P \\ P^T & 0 \end{bmatrix} \in \mathbf{R^{(N+1)x(N+1)}}$$

and the $N+1$ system can be rewritten in matrix form

$$H\alpha = \psi \tag{36}$$

with $\psi(\mathbf{x}_{N+1}) = 0$. The interpolation expansion coefficients can be found after matrix inversion

$$\alpha = H^{-1}\psi \tag{37}$$

These coefficients can be used to interpolate the data in three-dimensional space and to find derivatives at any point. The x-velocity of the fluid is found by taking the partial derivative of the basis function with respect to the x-direction.

$$\frac{\partial \psi(\mathbf{x}_i)}{\partial x} = \sum_{j=1}^{N} \alpha_j g_j'(\mathbf{x}_i) \tag{38}$$

Several basis functions were tested and compared before implementation in the code. Of the many functions available, the three shown below exhibit the quality of a "sphere of influence", such that points closer to the node of interest have a larger influence on that node

$$g_j(\mathbf{x}) = e^{-\frac{||\mathbf{x}-\mathbf{x}_j||}{c_j}} \quad \text{Exponential Spline} \tag{39}$$

$$g_j(\mathbf{x}) = e^{-\frac{||\mathbf{x}-\mathbf{x}_j||^2}{c_j^2}} \quad \text{Gaussian} \tag{40}$$

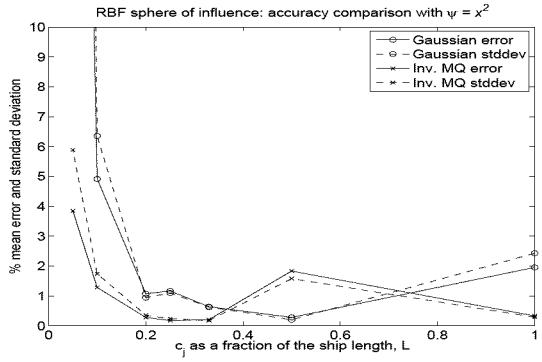

Figure 2: RBF c_j comparison

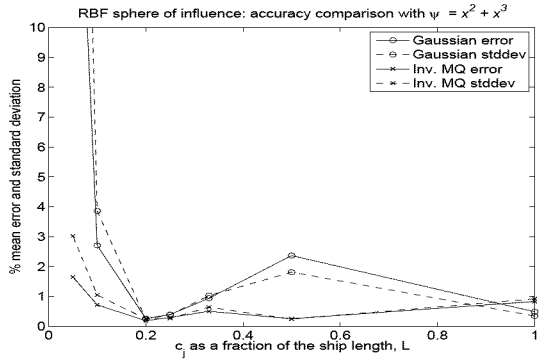

Figure 3: RBF c_j comparison

$$g_j(\mathbf{x}) = (1 + \frac{||\mathbf{x}-\mathbf{x}_j||^2}{c_j^2})^{-1/2} \quad \text{Inverse MQ} \tag{41}$$

Using a defined analytic velocity potential as a test, the candidate functions were compared in accuracy of interpolation and approximation to partial derivatives. The analytic potential was of the form $\psi \propto x^2$, with some variation for nodes on the same station (x-location). Another function, $\psi \propto x^2 + x^3$, was tested as well. The approximate partial x-derivatives were compared to the known solutions. The Gaussian equation (40) and Inverse Multi-Quadratic equation (41) proved to be the more accurate functions. Their accuracy depends on the "sphere of influence" term, c_j. Several tests cases were run to determine an the optimum value of this variable. They involved computing the partial x-derivative of the RBF approximation and comparing it to the known solution. Both the Gaussian and Inverse Multi-Quadratic functions were evaluated. Mean error and standard deviation were considered as benchmarks of comparison. The percentages (based on the mean absolute value of the exact solutions) of mean error and standard deviation are shown as functions of c_j in Figures 2 and 3. They indicate that using approximately $L/4$ yields good results for both functions.

Implementing this radial basis in the code resulted in occasional instabilities, especially for extreme am-

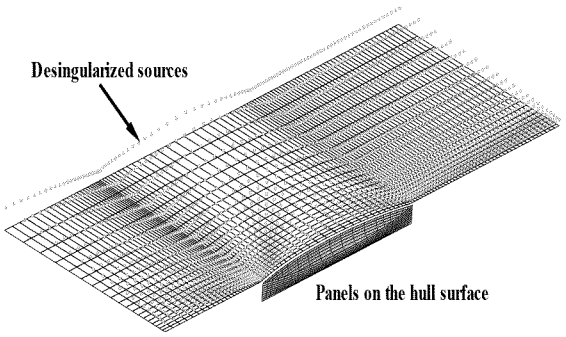

Figure 4: Desingularized sources distribution above calm water and flat panels discretization on the hull

plitude motions at higher frequency. The source of the instability is the $\partial\psi/\partial x$ term. It is a result of very high condition numbers in the matrix inversion routines, which use LU decomposition. Several attempts were made to correct this, but some instabilities remained. The Exponential Spline function, equation (39), although less accurate, had much smaller condition numbers. The final selection for use in the code was an exponential function of power 1.5, as shown in equation (42). This function was much more accurate than the Exponential Spline while being better conditioned for matrix inversion.

$$g_j(\mathbf{x}) = e^{-\frac{||\mathbf{x}-\mathbf{x}_j||^{1.5}}{c_j^{1.5}}} \tag{42}$$

The results were again verified against analytic velocity potentials. This RBF gives accurate approximations to $\partial\psi/\partial x$, while remaining stable when implemented in the real code under real conditions.

4 RESULTS AND DISCUSSION

Numerical convergence tests for both two-dimensional and three-dimensional problems have been shown in previous papers (Zhang and Beck, 2007; Zhang, 2007).

4.1 Three-Dimensional Results

Figure 4 shows the desingularized source distribution above the $z = 0$ and the flat panel distributions on a modified Wigley hull. Figure 5 and Figure 6 show the force time history results of the wave diffraction problem for a modified Wigley hull at $Fn = 0.3$ in head seas. The incident wavelength $\lambda/L = 1.0$, where L is the ship length of the modified Wigley hull; λ is the incident wave length; β is the angle of wave propagation measured from the positive sense of the x-axis.

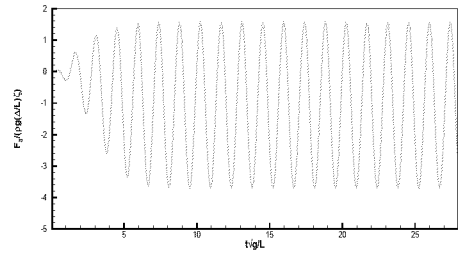

Figure 5: Diffraction force (heave force) acting on a Wigley hull III, $Fn = 0.3$, $\lambda/L = 1.0$, $\beta = \pi$

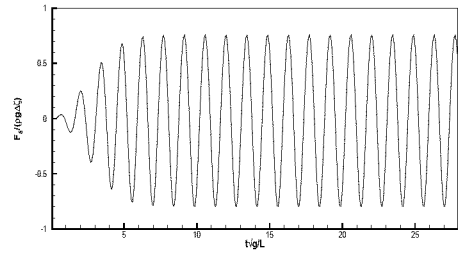

Figure 6: Diffraction force (pitch moment) acting on a Wigley hull III, $Fn = 0.3$, $\lambda/L = 1.0$, $\beta = \pi$

4.2 Two-Dimensional Strip Theory Results

Figures 7 through 10 show the force time series for forced heave motions of the S-175 containership. Positive heave displacement indicates the vessel is above it's calm water position. The particulars of the S-175 are given in Table 1. The simulations are for small and large amplitudes of heave, at low and high frequencies of oscillation. The simulations were run at zero and varying forward speeds corresponding to $Fn = 0.0, 0.15, 0.3$. The radiation force can be seen at these various speeds.

The pitching moment is most sensitive to forward speed. As expected, the radiated force is largest for the high frequency case. Non-linear behavior can be seen in the large amplitude motion, where the transom stern section of the body exits and enters the water. It is especially evident in the high frequency case, as can be seen in Figure 10.

Lpp(m)	175
B(m)	25.4
D(m)	15.4
T(m)	9.5
$\triangle$(t)	24742

Table 1: Parameters of S-175 hull

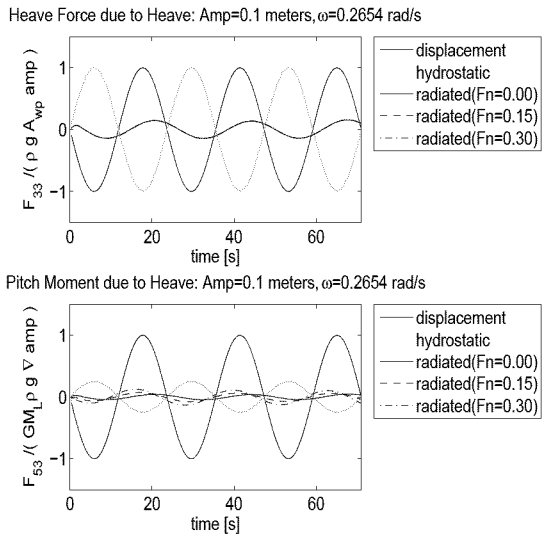

Figure 7: S-175 0.1 m forced heave at 0.2654 rad/s

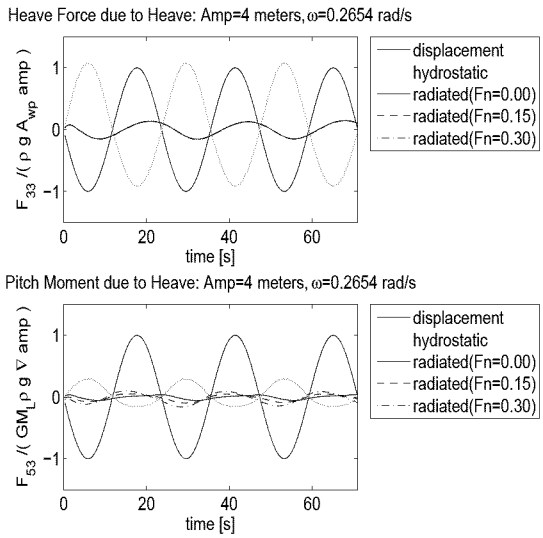

Figure 9: S-175 4.0 m forced heave at 0.2654 rad/s

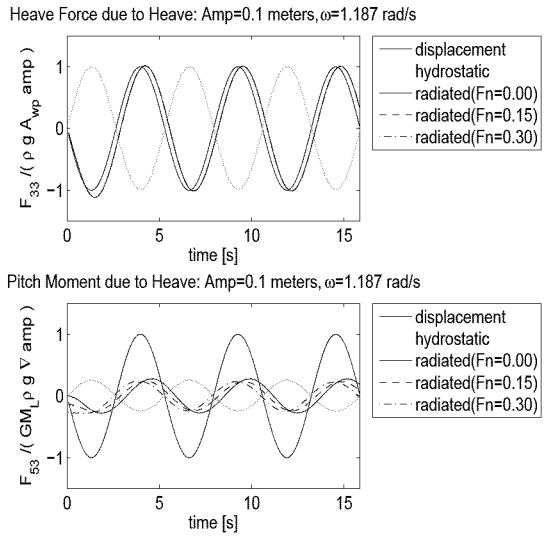

Figure 8: S-175 0.1 m forced heave at 1.1870 rad/s

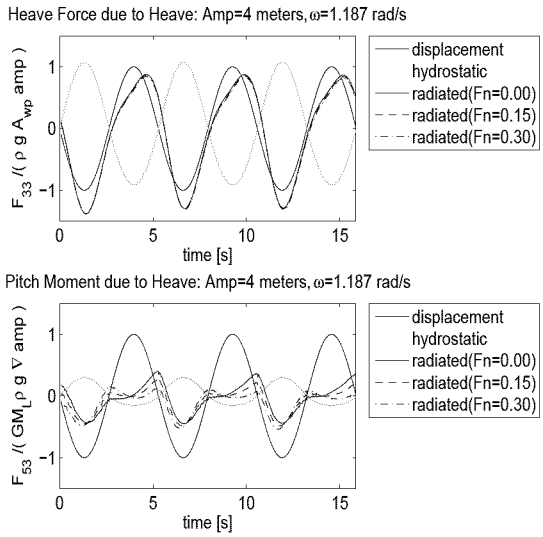

Figure 10: S-175 4.0 m forced heave at 1.1870 rad/s

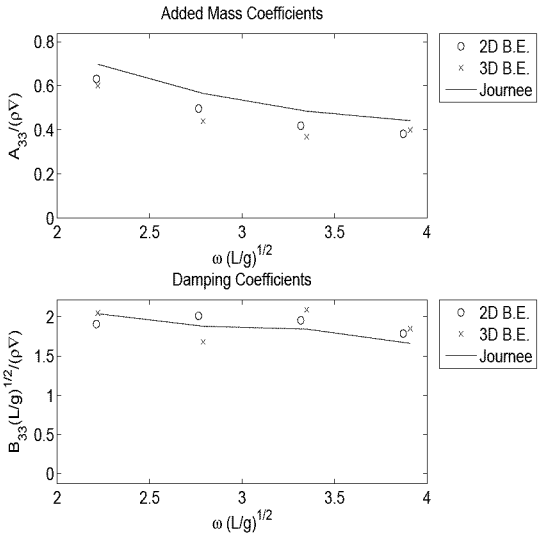

Figure 11: Wigley III Coefficients, Heave due to Heave

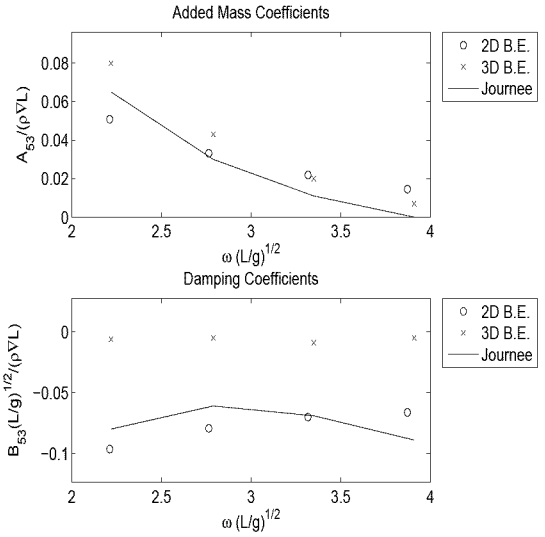

Figure 12: Wigley III Coefficients, Pitch due to Heave

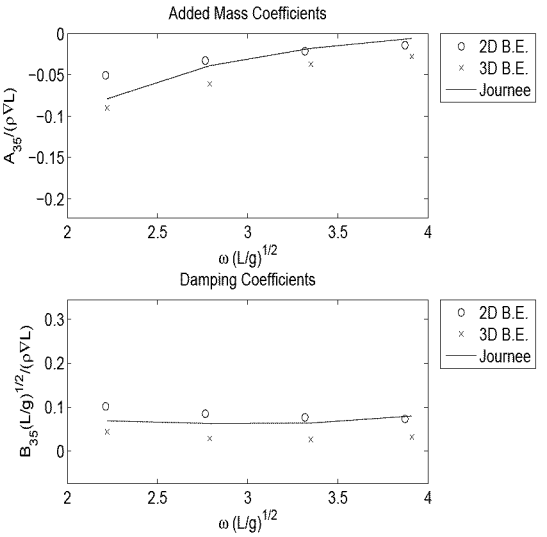

Figure 13: Wigley III Coefficients, Heave due to Pitch

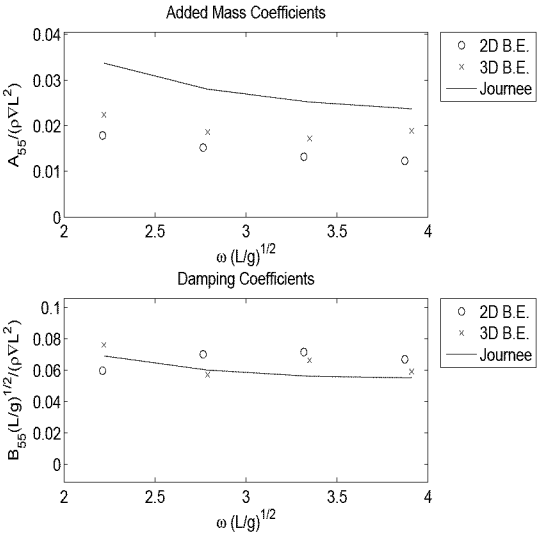

Figure 14: Wigley III Coefficients, Pitch due to Pitch

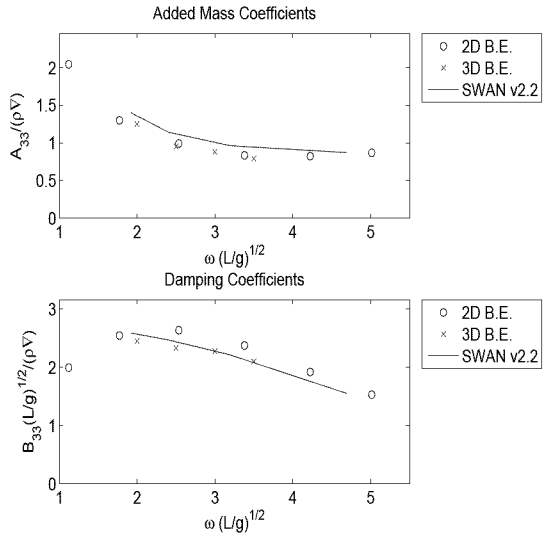

Figure 15: S-175 Coefficients, Heave due to Heave

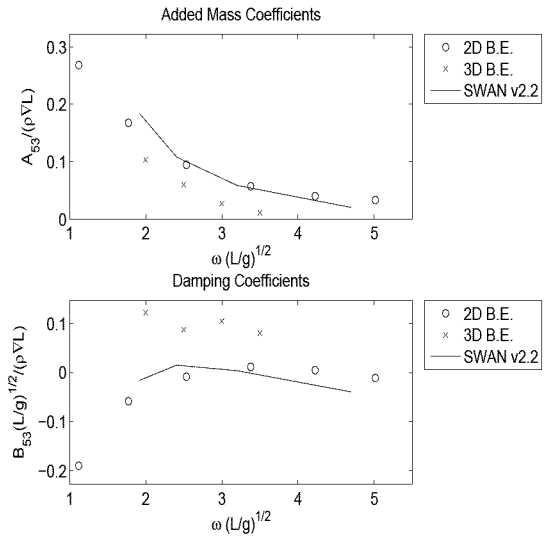

Figure 16: S-175 Coefficients, Pitch due to Heave

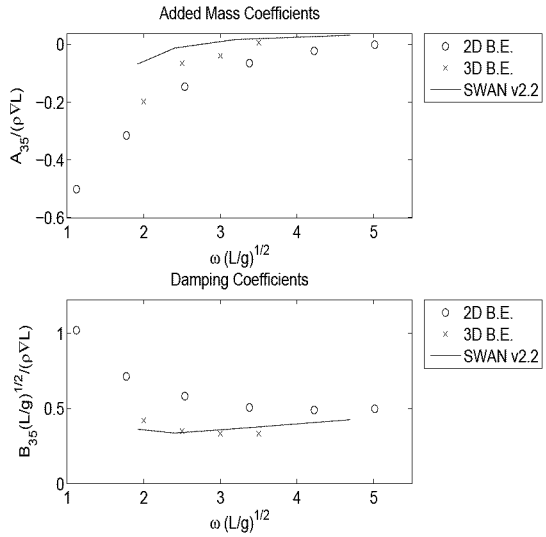

Figure 17: S-175 Coefficients, Heave due to Pitch

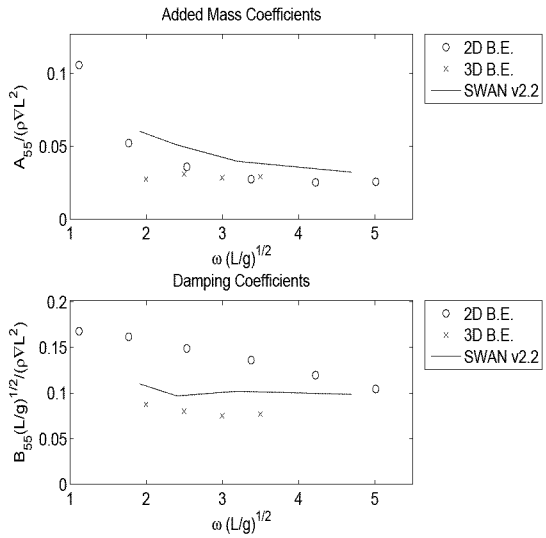

Figure 18: S-175 Coefficients, Pitch due to Pitch

4.3 Comparisons

Figures 11 through 14 display the heave and pitch added mass and damping coefficients for the modified Wigley hull at $Fn = 0.3$, due to heave and pitch motions. This modified Wigley hull corresponds to Journée's "Wigley III", as referenced in Journée (1992). Both the fully three-dimensional and two-dimensional strip theory codes were used and the results are compared the experimental results of Journée. Most of the coefficients compare well. The first exception is the damping in pitch due to heave, B_{53} in Figure 12. The three-dimensional results are high. The other exception is pitch added mass due to pitch, A_{55} in Figure 14. The current methods' values are low compared to experiments. This was found to be the case for most computational methods when comparing to Journée's findings for these coefficients.

Figures 15 through 18 display the added mass and damping coefficients for the S-175 containership in heave and pitch, due to heave and pitch motions. The simulations were performed with forward speed corresponding to $Fn = 0.275$. Both the fully three-dimensional and two-dimensional strip theory codes were used and the results are compared with SWAN version 2.2 as obtained by personal correspondence with Prof.Sclavounos. In general, the coefficients agree well. Again, an exception is the damping in pitch due to heave, B_{53} in Figure 16. These discrepancies are consistent with the modified Wigley hull findings. The two-dimensional results for forced pitch motions do not agree as well as they did for the case of the modified Wigley hull. Forward speed affects pitch motions more-so than heave motions, and the S-175 shows more non-linearities at the bow and stern.

4.4 Conclusions

Two-dimensional and three-dimensional body-exact computational models are formulated and developed in this paper. Numerical computations of the hydrodynamic coefficients for a modified Wigley hull and a S7-175 hull are compared with experiments and other numerical solutions. The comparison shows the capabilities and efficiency of the present two-dimensional and three-dimensional body-exact models. It is indicated by comparisons that three-dimensional free surface effects are more important in computing the hydrodynamic coefficients due to the pitch motion, while time domain strip theory can achieve relatively faster simulation.

The methods discussed here are similar in that they model the ship's orientation in the water exactly and utilize the time-domain approach. However, they are drastically different when solving interesting problems of surge and forward speed (i.e. calm water resistance). The three-dimensional approach inherently captures these details, while the two-dimensional requires some sort of forward speed correction term. The tradeoff is that the two-dimensional strip theory is computationally less expensive, typically by a factor of $8 \sim 10$.

5 ACKNOWLEDGMENT

This work was supported by Office of Naval Research, contracts N00014-04-1-0266 and N00014-05-1-0537.

References

Beck, R. F. and Magee, A. (1990). Time-domain analysis for predicting ship motions. In *Proc. IUTAM Symp., Dynamics of Marine Vehicles and Structures in Waves*, London, pp. 49–65.

Buhmann, M. D. (2000). Radial basis functions. *Acta Numerica*, 1–38.

Cao, Y. (1991). *Computations of nonlinear gravity waves by a desingularized boundary integral method.* Ph. D. thesis, The University of Michigan, Department of Naval Architecture and Marine Engineering.

Cao, Y., Lee, T. H., and Beck, R. F. (1992). Computation of nonlinear waves generated by floating bodies. In 7^{th} *International Workshop on Water Waves and Floating Bodies*, Val de Reuil,France, pp. 47–52.

Cao, Y., Schultz, W. W., and Beck, R. F. (1990). Three-dimensional, unsteady computations of nonlinear waves caused by underwater disturbances. pp. 417–427. 18^{th} Symposium on Naval Hydrodynamics.

Cao, Y., Schultz, W. W., and Beck, R. F. (1991). A three-dimensional desingularized boundary integral method for potential problems. *International Journal of Numerical Methods in Fluids 11*, 785–803.

Dommermuth, D. G. and Yue, D. K. P. (1987). Numerical simulations of nonlinear axisymmetric flows with a free surface. *J. of Fluid Mech. 178*, 195–219.

Hess, J. L. and Smith, A. M. O. (1964). Calculation of non-lifting potential flow about arbitrary three-dimensional bodies. *J. of Ship Research 8*(2), 22–44.

Journée, J. M. (1992). Experiments and calculations on four wigley hull forms,technical report 909. Technical report, Delft University of Technology, Ship Hydromechanics Laboratory, Delft, The Netherlands.

Kansa, E. J. (1999). Motivation for using radial basis functions to solve pdes. Technical report, Lawrence Livermore National Laboratory, Livermore, Ca.

Lee, T. H. (1992). *Nonlinear radiation problems for a surface-piercing body.* Phd thesis, The University of Michigan, Department of Naval Architecture and Marine Engineering.

Lin, W. M. and Yue, D. K. P. (1990). Numerical solutions for large-amplitude ship motion in the time domain. In *Proc.* 18^{th} *Symposium on Naval Hydrodynamics*, Ann Arbor, MI, pp. 41–66.

Longuet-Higgins, M. S. and Cokelet, C. D. (1976). The deformation of steep surface waves on water: I. a numerical method of computation. *Proc. of the Royal Society of London A350*, 1–26.

Newman, J. N. (1986). Distributions of sources and normal dipoles over a quadrilateral panel. *J. of Engineering Mathematics 20*(2), 113–126.

Scorpio, S. M., Beck, R. F., and Korsmeyer, F. T. (1996). Nonlinear water wave computations using a multipole accelerated, desingularized method. In *Proc. of the* 21^{st} *Symposium on Naval Hydrodynamics*, Trondheim, Norway, pp. 34–43.

Xue, M., Xu, H., Liu, Y., and Yue, D. K. P. (2001). Computations of fully nonlinear three dimensional wave-wave and wave-body interactions. part 1. dynamics of steep three dimensional waves. *J. of Fluid Mech. 438*, 11–39.

Zhang, X. S. (2007). *Large amplitude ship motion computations using a time dependent body geometry.* Phd thesis, The University of Michigan, Department of Naval Architecture and Marine Engineering.

Zhang, X. S. and Beck, R. F. (2006). 2-D body-exact computations in the time domain. In *Proc.* 21^{th} *International Workshop on Water Waves and Floating Bodies*, Loughborough, England, pp. 197–200.

Zhang, X. S. and Beck, R. F. (2007). Computations for large-amplitude two-dimensional motions. *J. of Engineering Mathematics (Special Volume in Honor of J.N. Newman).*